EES Batteries

Accepted Manuscript

This article can be cited before page numbers have been issued, to do this please use: D. Wu and K. B. Hatzell, *EES Batteries*, 2025, DOI: 10.1039/D5EB00097A.

View Article Online
DOI: 10.1039/D5EB00097A

As the world adds more renewable energy to the grid, there's a growing need for low-cost, long-duration energy storage—ideally at or below $20 per kilowatt-hour. Meeting this challenge requires moving beyond today's lithium-ion batteries. One promising option is sodium metal batteries. Sodium is far more abundant than lithium and can store a high amount of energy, making it an attractive alternative. To make these batteries both safe and efficient, researchers are exploring solid electrolytes materials that replace the flammable liquid components found in most batteries today. Solid electrolytes made of glass or ceramic could unlock safer, higher-energy sodium batteries. But a challenge associated with these materials is the necessesity for high operating temperatures (above 300°C), which drives up the cost of battery systems to around $300 per kilowatt-hour. This is currently far too expensive for widespread use. This paper discusses opportunities and challenges with room-temperature sodium metal batteries based on liquid metal. If successful, this technology could offer a safe, scalable, and affordable solution for storing renewable energy, helping us transition to a cleaner and more resilient power grid.

View Article Online
DOI: 10.1039/D5EB00097A

Chemo-Mechanical limitations of liquid alloy anodes for sodium solid-state batteries

Daren Wu[†] and Kelsey B. Hatzell[*,†,‡,¶]

†*Andlinger Center for Energy and the Environment, Princeton University, Princeton, NJ 08540, USA*

‡ *Department of Mechanical and Aerospace Engineering, Princeton University, Princeton, NJ 08540, USA*

¶ *Department of Chemical and Biological Engineering, Princeton University, Princeton, NJ 08540, USA*

E-mail: kelsey.hatzell@princeton.edu

Abstract

Sodium-potassium (NaK) liquid metal anodes address interfacial challenges in sodium solid-state batteries by eliminating solid-solid contact issues of solid Na anodes. *Operando* galvanostatic electrochemical impedance spectroscopy and *in situ* synchrotron X-ray computed tomography experiments reveals that interfacial Na depletion upon electrodissolution results in void formation and K metal precipitation. Conversely, Na plating upon electrodeposition results in local Na accumulation at the interface. Long-term deposition results in Na filament growth and short-circuit failure. These degradation processes arise from poor wetting due to the high surface tension of NaK and its limited Na diffusivity. Strategies which reduce the tendency for segregation are necessary for long-term cycling.

View Article Online
DOI: 10.1039/D5EB00097A

Introduction

Sodium solid-state batteries (SSSBs) are attractive candidates for large-scale, stationery energy storage applications due to the earth abundance of Na element, and high safety of non-flammable solid electrolytes.[1] In particular, the use of Na metal anode enable by solid electrolytes help increase the battery energy density to meet commercial application requirements.[2,3] Engineering challenges, however, persists with the anode-electrolyte interface in solid-state batteries, mainly due to the non-uniform solid-solid contact between alkali metal anodes and solid electrolytes.[4–6] The electrodissolution (stripping) and electrodposition (plating) of metal anodes result in various chemo-mechanical effects including volumetric variations, stress buildup and interfacial void formation. Those effects lead to metal filament growth and penetration failure of the solid electrolyte.[7–12]

Sodium-potassium (NaK) alloys as a room-temperature liquid anode was proposed for addressing this anode-electrolyte interface challenge.[13,14] Under room temperature, the liquid phase of NaK alloys will be thermodynamically maintained over a wide compositional window ($\sim$44 wt% K to $\sim$ 88 wt% K),[15–17] theoretically allowing Na stripping and plating activities without precipitation of any solid metal, effectively preventing Na metal accumulation and filament growth. However, thermodynamic predictions do not accurately reflect NaK's response under applied Na stripping/plating currents, when kinetic factors may dominate and thermodynamic predictions are no longer valid. Under cycling current, local Na depletion or enrichment at the anode-electrolyte interface may lead to liquid-solid phase separations (precipitation of Na metal or K metal). Therefore, understandings in the chemo-mechanical limitations of this liquid anode under operating conditions is critical. Previous studies on NaK liquid anodes, however, commonly utilized carbon additives[18] or porous carbon substrates[13,14,16] to modify mechanical properties of NaK alloys. These modifications enables fabrication of self-standing liquid NaK anodes for battery assembly but at the same time altered the the chemo-mechanical properties of NaK. The strong chemical and physical interactions between NaK liquid and carbon[19,20] reduces their fluidity, thus the electrochemical

View Article Online
DOI: 10.1039/D5EB00097A

response of these modified NaK anodes are not reflective of the properties of pure liquid NaK alloys.

In this work, we studied the chemo-mechanical limitations of pure liquid NaK anodes paired with sodium superionic conductor ($Na_3Zr_2Si_2PO_{12}$, NASICON) solid electrolytes. *Operando* galvanostatic electrochemical impedance spectroscopy (GEIS) collected during Na stripping/plating of NaK liquid anodes show that the stripping and plating processes have different kinetic limitations due to different interfacial chemo-mechanical degradations triggered by current. Pulsed Na stripping experiments and *In situ* X-ray computed tomography (XCT) imaging experiment performed during Na plating process help elucidate the fundamental mechanism behind the unstable cycling behavior of pure liquid NaK anodes. We conclude that 1) Na stripping from NaK becomes unstable under high current due to the developing Na concentration gradient near the anode-electrolyte interface, which triggers voiding and K metal precipitations that significantly increases interfacial resistance. 2) Na plating into Na can result in interfacial Na metal accumulation under high plating current or repeated stripping-plating cycles. Continued Na plating under these conditions leads to Na filament growth and short-circuit failure. Our results suggest that the electrochemical performance and stability of NaK liquid metal anodes are limited by the combined effect of its high surface tension and Na mobility. High surface tension results in insufficient wetting between NaK and solid electrolytes, limiting the electrochemical active area; the resultant current focusing effect drives interfacial Na depletion that cannot be compensated by Na diffusion inside NaK, leading to chemo-mechanical degradations.

Experimental Methods

Preparation of Na-K liquid anodes: Na-K alloys with 50, 65 and 80 wt% K (NaK50, NaK65 and NaK80) was prepared by placing Na and K metal chunks of desired weight ratios in a glass vial together then shook vigorously until a uniform liquid metal bulb forms.

View Article Online
DOI: 10.1039/D5EB00097A

Preparation of (NASICON) solid-state electrolyte: Commercial $Na_3Zr_2Si_2PO_{12}$ powder (MSE Supplies) was cold pressed at 625 MPa then sintered at 1230°C for 12 h with a ramping rate of 5°C/min to form self-standing electrolyte pellets with a thickness of ∼1.5 mm. A 20 nm SnO_2 coating was applied to the as-sintered NASICON pellet surface that's going to contact NaK based on the procedure reported previously.[21] 20 nm of Sn metal was first sputtered onto NASICON surface using a VCR IBS/TM200S Ion Beam Sputterer, then transferred to a tube furnace and annealed at 900 C for 3 h to form SnO_2. Upon contact with NaK liquid anodes, this SnO_2 layer transforms into a ion-electron conductive layer K_2O/K_xSn,[22] which acts as a selective interface to block K ions and conduct Na ions,[23] thus enables cycling of NaK anodes.

Assembly of solid-state electrochemical cells: For Na metal cells, Na metal chunks were rolled into foils and disks with a diameter of 8 mm were cut from the foils then stuck onto ϕ10 mm Cu foil current collectors. Surface of Na metal was mechanically cleaned before attaching to NASCION electrolyte. NaK/NASICON/Na asymmetric cells were assembled between 10 mm stainless steel plungers inside PEEK-lined stainless steel cell body. A spring-loaded pressure frame was used to apply 10 MPa external pressures to the whole cell for Na metal electrode to form a low-resistance Na/NASICON interface. A rubber O-ring with 10 mm outer and 7 mm inner diameters were used on the NaK liquid electrode side to provide seal and confine liquid NaK. 40 μL of NaK liquid was dropped inside the O-ring to form a liquid metal chamber upon cell assembly. For all asymmetric cells assembled for impedance measurements, Na quasi-reference electrodes (Na-QREs) are prepared according to previously reported procedure.[24] Na/NASICON half cell stack was first assembled & vacuum-sealed inside plastic pouches, then transferred to an isostatic press for pressing under 100 MPa for 15 mins to form a zero-resistance Na/NASICON interface (Figure **??**).

Electrochemical testing: Critical current density (CCD), pulsed stripping and electrochemical Impedance Spectroscopy (EIS) and galvanostatic cycling tests were performed with BioLogic SP-300 and VMP-3 potentiostats. The frequency range of EIS tests was 7 MHz to

View Article Online
DOI: 10.1039/D5EB00097A

5 Hz. For *in-situ* galvanostatic EIS (GEIS) tests, electrochemical cells were cycling under a constant current, with GEIS being continuously collected at 5 μA amplitude perturbations. Staircase GEIS (SGEIS) experiments were conducted between 0.05 - 1 mA/cm^2 current densities, either for Na stripping or Na plating on NaK working electrodes, with a current step size of 0.01 mA/cm^2. For each current density, a constant current was first applied for 5 s, followed by GEIS measurement at 5 μA amplitude, which takes $\sim$35 s to complete, resulting a 40 s step duration. Collected EIS data was processed and analyzed with Relaxis software package. For distribution of relaxation time (DRT) analysis, both the real part and imaginery part of EIS data were used for DRT transformation, with a regularization parameter λ of 10^{-3} .

Synchrotron in situ X-ray computed tomography experiments: A custom designed cylindrical PEEK cell with 6 mm inner diameter was used for *in situ* synchrotron X-ray computed tomography experiments conducted at the 27-ID HEX beamline[25] at National Synchrotron Light Source II, Brookhaven National Laboratory. For the *operando* cells, a rubber O-ring with 6 mm outer diameter and 4 mm inner diameter was used to seal NaK liquid anode between the NASICON electrolyte and Al current collector. An external pressure of $\sim$10 MPa was applied by adjusting the torque of cell tightening screws. Monochromatic X-ray beams at 80 keV was directed to the cell and the transmitted beams were converted to visible light by a scintillator, then collected by a CCD camera to obtain a single radiography image with a 4 $\times$ 4 mm field of view and 1.3 μm pixel size. For each tomography image, 3001 radiography projections were collected with an exposure time of 0.2 s each over a 180° cell rotation. The raw projection images were processed using the Algotom software,[26] which includes the following data processing workflow: flat-field normalization, center-of-rotation determination, zinger removal, ring artifact removal,[27] and filtered back-projection.

View Article Online
DOI: 10.1039/D5EB00097A

Results and discussion

Unstable cycling behavior of NaK liquid anodes

Critical current density (CCD) testing on NaK50 reveal cell short-circuited during Na plating at 0.4 mA/cm^2 (Figure 1a). At lower current densities (0.05 and 0.1 mA/cm^2), Na stripping and plating showed stable voltage profiles. As the current increased above 0.2 mA/cm^2, the steadily rising voltage during Na stripping indicates a growing charge transfer resistance. This trend is also evident in the *operando* DRT spectra collected during the CCD test (Figure 1b–e; the original EIS spectra are provided in Figure **??**.). These spectra, plotted as logarithmic-scale contour plots with color representing resistance $\gamma(\Omega)$, show two peaks at 0.05 and 0.1 mA/cm^2. The two peaks represent the grain boundary resistance in the NASICON electrolyte (γ_{GB})[24] and interfacial resistance (γ_{int}) at the NaK/NASICON interface (Figure 1b). The interfacial resistance (γ_{int}) arises from two main factors: (1) mechanical constriction caused by micro- or nano-scale voids at the NaK/NASICON interface, due to the high surface tension of the NaK alloy,[28–30] and (2) charge transfer resistance between NaK and the NASICON electrolyte.[31] By contrast, in a Na/NASICON/Na symmetric cell, mechanical constriction can be minimized through uniaxial or isostatic pressing, resulting in near-ideal interfacial contact and a negligible γ_{int} (Figure **??**).[24]

Both γ_{GB} and γ_{int} remained nearly constant during cycling at 0.05 and 0.1 mA/cm^2, indicating that the NaK/NASICON interface remained stable. The γ_{int} peak increased and broadened during liquid metal stripping at 0.2 mA/cm^2, indicating either enhanced mechanical constriction (e.g., void formation or enlargement) or increased charge transfer resistance (Fig. 1d). The γ_{int} decreased when the current was reversed and Na was plated into the liquid metal anode. The decrease in γ_{int} indicates improved NaK/NASICON interfacial contact during deposition (Figure 1d, e).

γ_{int} rapidly diminished and eventually vanished during plating at 0.4 mA/cm^2, suggesting that Na metal deposition filled pre-existing pores and enhanced the NaK/NASICON inter-

View Article Online
DOI: 10.1039/D5EB00097A

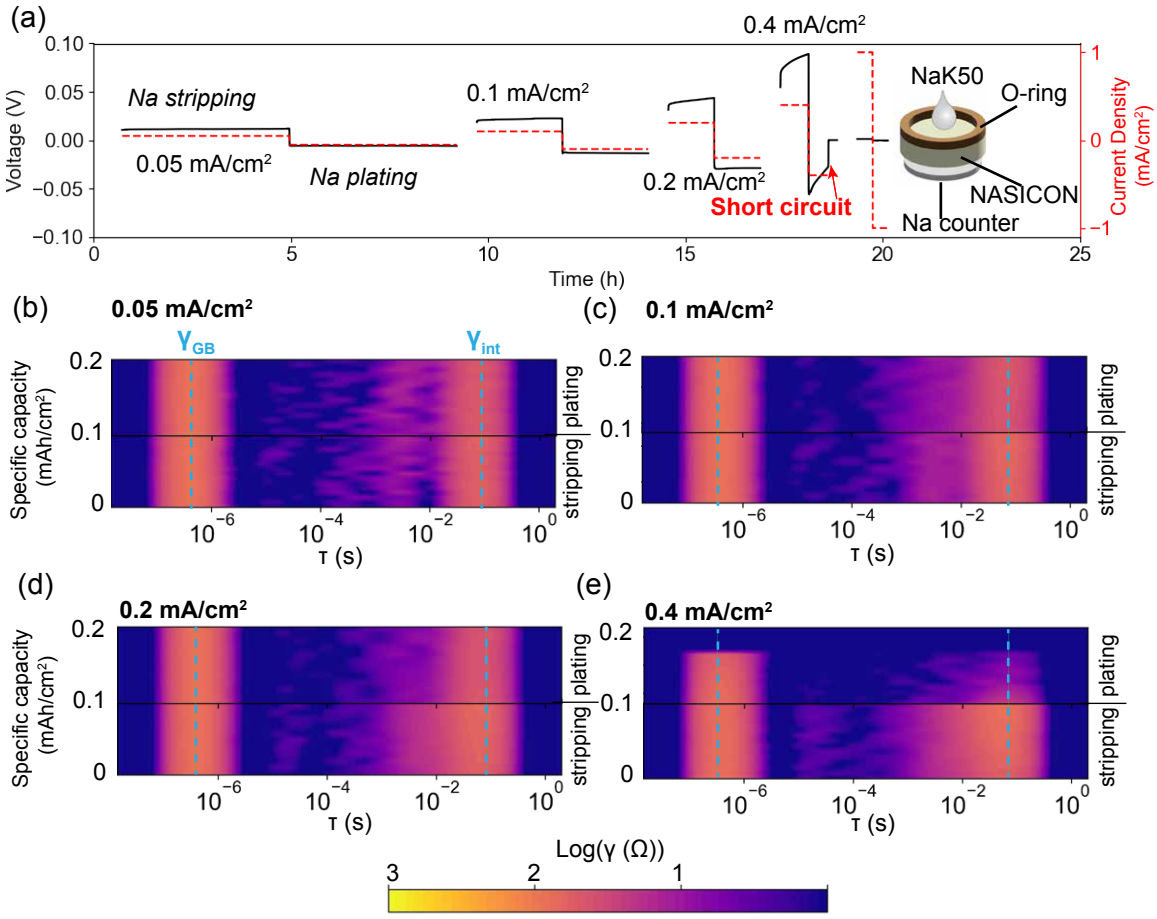

Figure 1: (a) Critical current density test on liquid NaK50 working electrode, with constant GEIS measurement (∼35 s per GEIS scan during cycling). (b – e) Distribution of relaxation time (DRT) spectra converted from GEIS spectra collected during the CCD test at different current densities.

facial contact (Figure 1d, e). Concurrently, γ_{GB} γ_{int} suddenly disappeared during plating, indicating mechanical failure of the NASICON pellet due to Na metal penetration .

red

In situ X-ray computed tomography (XCT) imaging during Na plating (at 0.7 mA/cm^2) into NaK liquid electrode short-circuited after only ∼ 0.5 mAh/cm^2 (Figure 2a,b). In contrast, *in situ* Na plating in NaK XCT at lower current densities (0.4 mA/cm^2, Figure **??**) proceeded without short-circuit, reaching 4 mAh/cm^2 cutoff capacity (Figure **??**a-c). *In situ* XCT cross-sections collected throughout this plating process demonstrated a characteristic edge-chipping fracture mechanism.[11,32,33] This has been previously shown with lithium solid

View Article Online
DOI: 10.1039/D5EB00097A

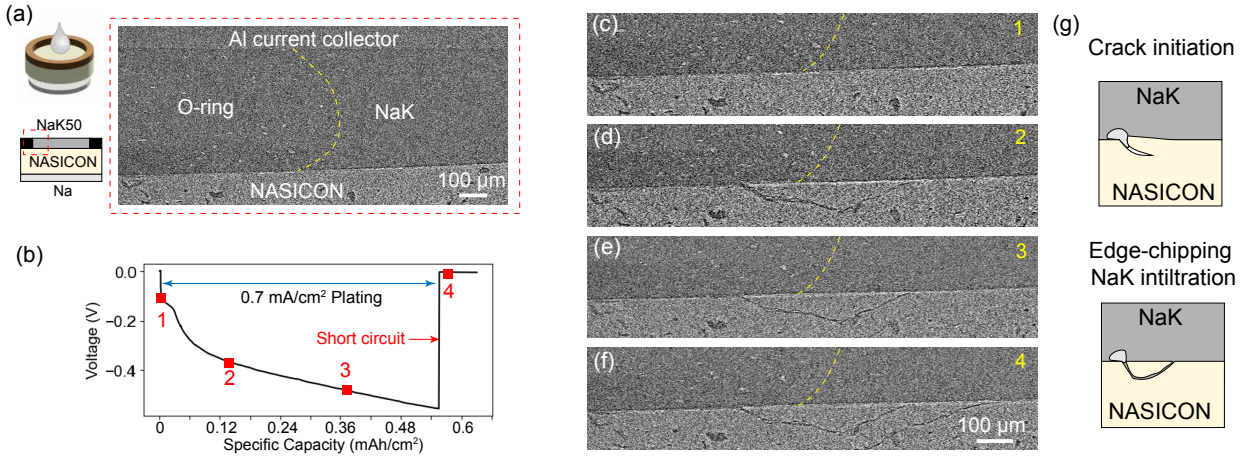

Figure 2: (a) Schematics of the *in situ* NaK/NASICON/Na cell assembled with an O-ring for *in situ* synchrotron XCT experiment and reconstructed virtual cross-section of of the region of interest (red dashed box) showing the cell components and active NaK/NASICON interface. (b) Voltage profile of *in situ* XCT cell during Na plating process of NaK liquid anode under 0.7 mA/cm^2 current density. (c-f) Reconstructed *in situ* XCT virtual cross-sectional images at the NaK/NASICON interface collected during Na plating process. Crack initiation-propagation inside NASICON that led to short circuit can be observed. (g) Illustration demonstrating the crack initiation-edge chipping process, with NaK infiltration after edge-chipping.

state batteries and attributed to high local current densities attributed to incomplete contact at an interface[11,32] (Figure 2c-f). The crack propagated quickly and eventually led to short-circuit with the cell voltage dropped to near 0 V (Figure 2b, f).[34–36] Although due to spatial resolution limits, sub-micron interfacial Na metal accumulation is not directly visible in the XCT images, the observed NASICON electrolyte fracture can only be caused by Na metal filament growth, as illustrated in Figure 2(g). As Na plating leads to interfacial Na metal precipitation at the NaK/NASICON interface, subsequent Na filament growth opens up a crack on the NASICON surface. With continued Na plating, the surface crack develops and eventually chips off a small piece of the NASICON electrolyte, allowing liquid NaK to infiltrate the crack. This electrolyte edge-chipping relieves some surface stress induced by Na filament intrusion, and the infiltrated NaK contacts and partially dissolves the Na filament. This combined phenomenon effectively reduced the crack size, as observed in the XCT images after edge-chipping (Figure 2(e-f)). The *in situ* XCT results confirm that liquid-solid

View Article Online
DOI: 10.1039/D5EB00097A

phase separation, in the form of Na metal precipitation, develops at the NaK/NASICON interface during Na plating, especially under high current densities. Note that from our previously published results, Na/NASICON/Na symmetric cell demonstrated a CCD of ∼3.2 mA/cm^2.[37] This previous result, combined with the XCT observations here, confirm that the short circuit phenomenon observed in Figure 1 is caused by the NaK liquid electrode, not the Na counter electrode.

Origin of unstable Na stripping behavior

To understand the unstable Na stripping behavior of the NaK/NASICON interface, we also performed *in situ* XCT imaging during staircase stripping of NaK liquid electrode (Figure **??**). The NaK50 working electrode went through Na stripping under 0.2, 0.4, 0.7 and 1 mA/cm^2 current densities, where unstable stripping behavior becomes apparent when the current density went above 0.7 mA/cm^2 (Figure **??** (a)). By comparing the reconstructed virtual cross-section images of the pristine state and under 1 mA/cm^2 stripping current (Figure **??** (b)), we observe the enlargement of a pre-existing bubble within the liquid NaK electrode as a direct result of Na stripping. This bubble, however, locates inside the NaK liquid, thus its enlargement does not directly contribute to interfacial resistance. No other interfacial evolutions are observable from the XCT images. This suggests that the length scales of the interfacial evolutions that resulted in unstable Na stripping behavior are smaller than the spatial resolution of the XCT beamline. Alternative interfacial probing method is needed to gain insights into this behavior.

Staircase GEIS (SGEIS) experiment was performed on NaK liquid working electrode against a Na reference (Figure 3 , original EIS spectra are provided in Figure **??**). This measurement mimics a linear current scanning experiment for probing the NaK anode response as a function of Na stripping current density, with an equivalent current scanning rate of ∼0.001 μA/s. The current scanning process revealed notable DRT changes, which rapidly recovered upon resting, followed by gradual relaxation and continued recovery over

View Article Online
DOI: 10.1039/D5EB00097A

the extended rest period (Figure 3b). A stable Na stripping regime, exhibiting relatively low voltage and a DRT spectrum dominated by γ_{GB} and a single γ_{int} peak near $\tau = 10^{-1}$ s, is observed over the current density range of 0 to approximately 0.6 mA/cm^2 (Figure 3a). Na atoms are steadily oxidized at the NaK/NASICON interface with a relatively low resistance. When stripping current goes above 0.6 mA/cm^2, however, the NaK working electrode enters an unstable stripping regime, with quickly rising cell voltage (Figure 3b) and changes in the DRT profile. First, as the current density increased, γ_{int} not only grew in magnitude but also shifted toward lower τ values, indicating shorter relaxation times. Second, a new peak appeared at $\tau = 10^{-4}$ to 10^{-3} s (γ'_{int}, Figure 3b), suggesting the onset of a new interfacial process with sub-millisecond relaxation time at higher stripping current densities. The increasing γ_{int} and γ'_{int} with increasing current density directly resulted in the non-linear voltage rise in the unstable Na stripping regime. SGEIS (current scanning) procedure ended after the GEIS measurement at 1 mA/cm^2 completed, the cell then entered an OCV resting period with continuous PEIS measurements taken at 35 s interval. By overlaying the last DRT spectra during SGEIS procedure (1 mA/cm^2/0 s upon resting) to DRT spectra taken at different resting times (Figure 3c), we examined the evolution of each DRT component as a function of resting length. In the first DRT spectra taken immediately after SGEIS completed (35 s into rest), γ_{int} shifted back to its original relaxation time (10^{-1} s) with increased amplitude, γ'_{int} completely vanished, meaning that the interfacial feature corresponding to γ'_{int} recovers completely within 35 s after stripping current stopped.

Increasing the potassium content in the NaK metal can increase the elasticity of the electrode. In practice, when an electrode is infinitely elastic contact should be maintained. The voltage profiles for NaK50, NaK65 and NaK80 during current scanning shows that the current threshold for unstable Na stripping behavior has strong NaK composition dependence. NaK65 entered unstable regime at $\sim$ 0.15 mA/cm^2, much lower than the $\sim$ 0.6 mA/cm^2 threshold observed for NaK50 (Figure **??**a). The *operando* DRT profile of NaK65 over the current scanning demonstrate slightly different behavior than NaK50 (Figure **??**c),

View Article Online
DOI: 10.1039/D5EB00097A

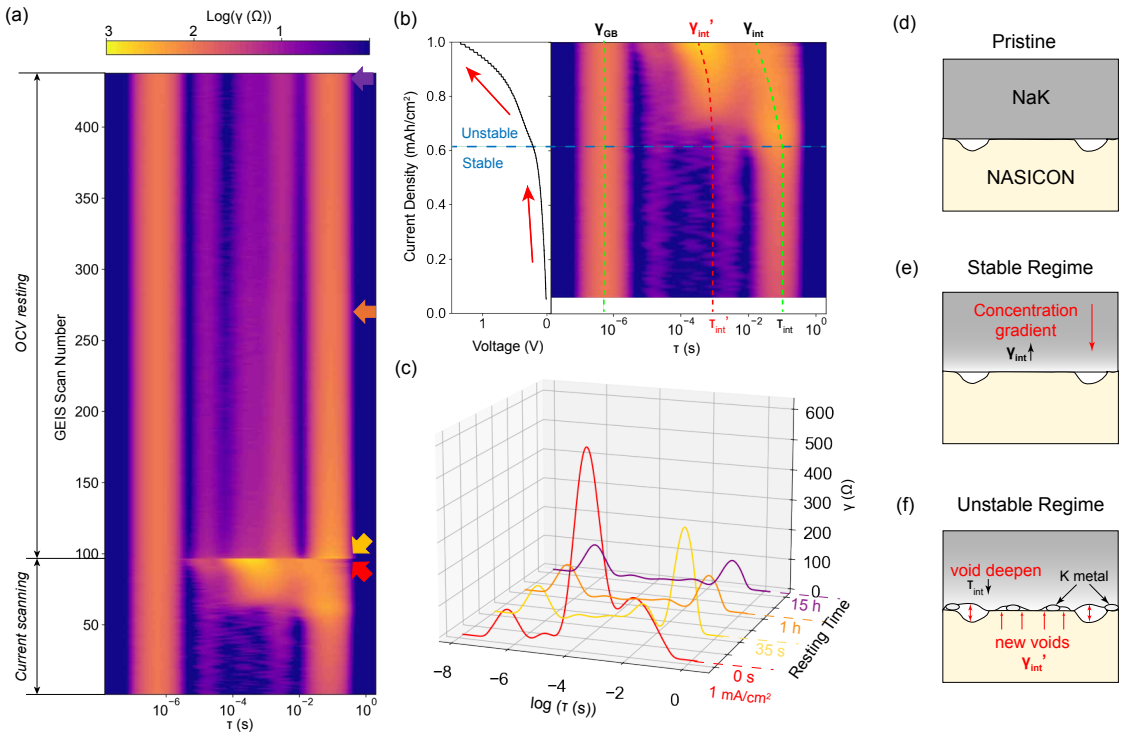

Figure 3: (a) *Operando* DRT spectra obtained during Na stripping SGEIS (current scanning) experiment on NaK50 liquid working electrode, followed by an extended resting period. (b) The voltage profile of the SGEIS test and corresponding DRT spectra as functions of Na stripping current density. (c) DRT spectra overlay during the OCV resting period. Schematics of the NaK/NASICON interface at (d) pristine state, and in (e) stable Na stripping regime, (f) unstable Na stripping regime.

which is better visualized in 3D DRT overlay plots (Figure **??**d, e). As Na stripping current approaches the unstable threshold for NaK65, γ_{int} shifted significantly toward lower τ value, and eventually merged with the newly emerged γ'_{int} at τ=10^{-3} s. (Figure 3e). As Na content goes lower with NaK80, the cell voltage of NaK80 during SGEIS quickly reached voltage limit (3 V) during the first GEIS measurement at 0.05 mA/cm^2 (Figure **??**), providing no complete EIS spectra.

Such composition dependence suggests that the starting Na content of NaK liquid anodes dictates the limiting current for Na stripping, which should be directly related to the Na concentration gradient that develops near the NaK/NASICON interface during stripping, similar to the mass transfer phenomenon studied in liquid electrolyte-electrode interfaces.[38] For Na oxidation reaction process ($Na - e^- \rightarrow Na^+$), the charge transfer resistance is

View Article Online
DOI: 10.1039/D5EB00097A

inversely proportional to the Na concentration ($R_{ct} \propto 1/C_{Na}$)at the interface.[38] Reducing interfacial Na concentration leads to significantly increased R_{ct}, reflected as increasing γ_{int} in the DRT spectra collected on pristine NaK/NASICON/Na cells with NaK50, NaK65 and NaK80 working electrodes (Figure **??**). Therefore, interfacial Na depletion accompanied by Na concentration gradient development directly result in increased γ_{int}, which dominates the observed DRT configuration within stable Na stripping regime (Figure 3e).

The emerging γ'_{int} within unstable Na stripping regime of both NaK50 and NaK65 should correspond to other chemo-mechanical interfacial evolutions triggered by drastically reduced interfacial Na content in NaK. Chemically, local Na depletion directly leads to precipitation of K metal, as suggested by Na-K phase diagram.[15] Na depletion and K precipitation generates additional K/NASICON interfaces and small interfacial voids (Figure 3f), effectively forming small, scattered mechanical constrictions that has a faster relaxation time than pre-existing voids (Figure 3d), accounting for γ'_{int} emerged at $\tau 10^{-3}$ s. Loss of Na metal at the NaK/NASICON interface could also directly deepen the pre-existing interfacial voids, leading to higher constriction capacitance with shorter relaxation time, shifting γ_{int} to smaller τ values.[28,39] For solid metal anodes in SSBs, void formation upon stripping due to insufficient metal diffusion and deformation is well-studied, characterized by increased interfacial/charge transfer resistance.[39,40] However, mechanical behavior of liquid metals like NaK are drastically different from solids. Their deformation/recovery time upon imposing/removing mechanical, electrical or electrochemical perturbations are typically in the ms regime ($\tau 10^{-3}$ s) with case studies on liquid metals actuators like mercury and gallium.[41–44] Particularly, in the case of electrochemically-induced mechanical deformation, previous report on liquid gallium-indium alloys observed that mechanical movement does not initiate until applied electrochemical current reaches a critical threshold,[45] which resembles the SGEIS results above, where DRT peak only shifts to or emerges at $\tau 10^{-3}$ s under high current. As the stripping current stopped, DRT spectra immediately recovers to near-pristine state, dominated by γ_{GB} ($\tau 10^{-6}$ s) and γ_{int} ($\tau 10^{-1}$ s), suggesting the interfacial degradations induced

View Article Online
DOI: 10.1039/D5EB00097A

by high Na stripping current recovers in under 35 s. (Figure 3c) The increased amplitude of γ_{int} between 0 s and 35 s upon resting could be due to the merging of smaller voids, as part of the mechanical recovery process. Between 35 s and 15 h resting period, the amplitude of γ_{int} gradually diminished to near-pristine state. The slower recovery process can be related to recovery of Na concentration gradient and liquid-solid phase separation, which require further experimental examination.

To summarize, the SGEIS-OCV experiment results demonstrate the reversible, dynamic chemo-mechanical degradation process of the NaK/NASCION interface during Na stripping, dominated by stripping current density. Under high Na stripping current, Na concentration gradient develops at the interface, and fast Na depletion leads to increased interfacial voiding, potentially accompanied by precipitation of K metal. Once the Na stripping current stops, a mechanical recovery process initiates. This process involves liquid flow, Na diffusion inside NaK, and re-dissolution of precipitated K metal, and the majority of these processes occur in under 35 s after the stripping current stops. The liquid flow re-compensates the interfacial voids, and Na diffusion homogenizes the Na concentration inside NaK until all K metal dissolves, and Na concentration gradient recovers. After the mechanical recovery, the NaK/NASICON interface return to near-pristine state, especially given that the total Na stripping capacity during the SGEIS experiment (< 1 mAh/cm^2) is much smaller than the theoretical capacity of the whole liquid NaK electrode (> 40 mAh/cm^2) based on its volumetric loading.

As the time resolution of *operando* GEIS experiments are limited to the duration of a single GEIS scan ($\sim$35 s), those experiments may not comprehensively capture interfacial processes that develop and recovers within shorter time frames during Na stripping from NaK. Pulsed stripping experiments, in this case, probes interfacial recovery behavior upon stripping with sub-second temporal resolutions (Figure 4a). In this experiment, a 1 s Na stripping current pulse at 1 mA/cm^2 current density imposed on NaK liquid anode is followed by a resting period ranging from 0.1 s - 10 s. Na stripping continues until the cell voltage

View Article Online
DOI: 10.1039/D5EB00097A

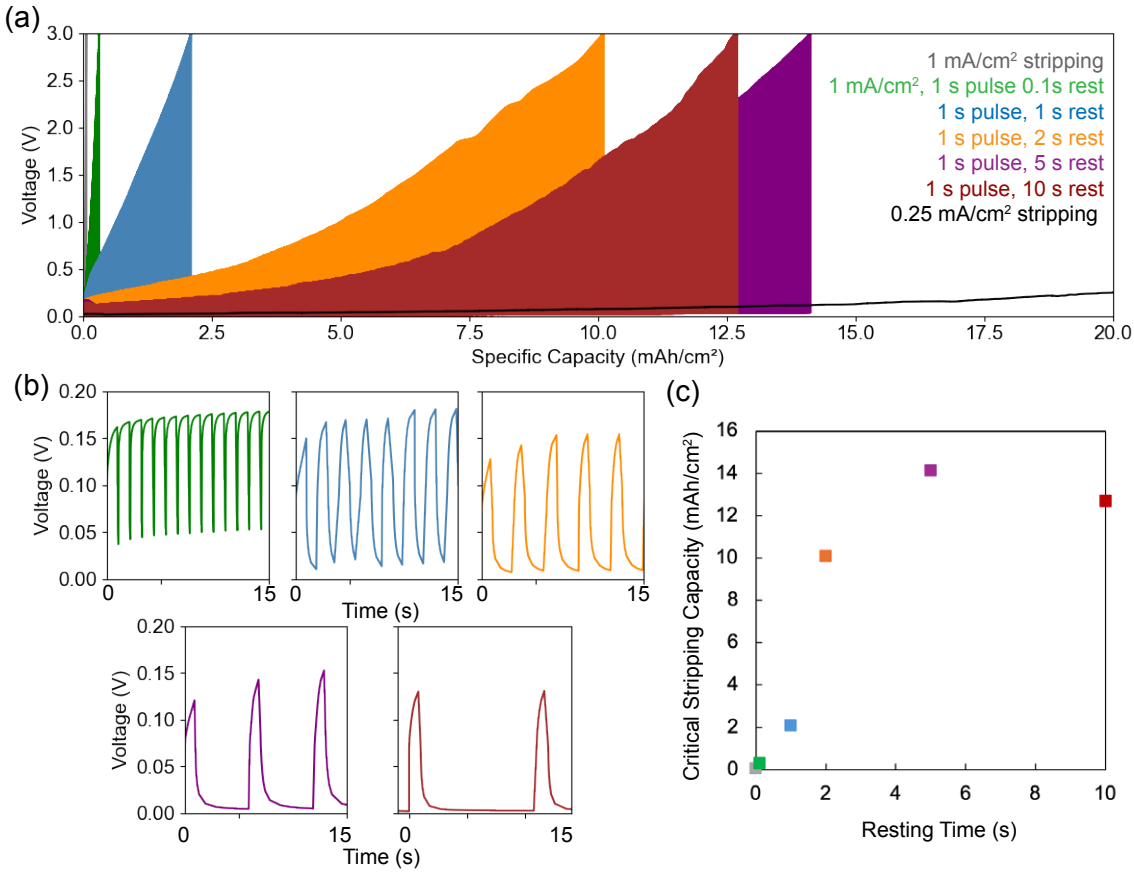

Figure 4: (a) Voltage curves of pulsed Na stripping experiment performed on NaK50 liquid anodes with different resting periods (0.1 - 10 s) after each 1 s current pulse. (b) Magnified voltage curves demonstrating the response of NaK anodes during current pulse-OCV resting cycles. (c) Critical stripping capacity of NaK anodes as a function of resting period length between current pulses. The theoretical critical stripping capacity under this experimental setup is ~40 mAh/cm^2.

reaches 3 V. The length of resting period, in this case, significantly impacts the critical stripping capacity of NaK working electrodes. With resting lengths between 0.1 - 2 s, the cell voltage continuously decreases during rest; it takes at least 5 s of resting time for the cell voltage to plateau after a 1 s current pulse. (Figure 4b) The critical stripping capacity of NaK liquid anode is directly affected by the resting length (Figure 4c). Direct stripping under 1 mA/cm^2 leads to very fast voltage increase and the NaK anode delivered minimal capacity. By introducing a 0.1 resting period after each 1 s current pulse, the NaK anode delivered slightly higher capacity. Extending the rest to 1-2 s yields a sharp increase in critical stripping capacity (~2 mAh/cm^2 to ~10 mAh/cm^2), whereas longer rests of 5-10

View Article Online
DOI: 10.1039/D5EB00097A

s show no further improvement, plateauing at 12-14 mAh/cm^2. This behavior indicates that the reversible component of interfacial chemo-mechanical degradation induced by Na stripping fully recovers within ∼5 s after the current stops. Given the capacity trend in Figure 4, we can infer that the recovery timescale is roughly 2-5 s, as the capacity reaches a plateau somewhere between 2 s and 5 s resting times. In contrast, under a lower current density (0.25 mA/cm^2), the cell voltage remains low up to the cutoff capacity (20 mAh/cm^2), suggesting that slower interfacial degradation processes may require longer than 10 s to recover.

As discussed above, liquid metal deformation and recovery is on ms timescale. The fact that resting period of 0.1 s only slightly increased critical stripping capacity suggests that pure mechanical deformation contributes very little to the mechanical constrictions observed in DRT under high current. During Na stripping, the applied current creates a local Na^+ flux at the NaK/NASICON interface, which establishes a concentration gradient according to Fick's first law ($J = -D\partial C/\partial x$). The development and relaxation of this diffusion layer follow Fick's second law ($\partial C/\partial t = D\partial^2 C/\partial x^2$) with a characteristic timescale $t \sim L^2/2D$ (where L is the length of the diffusion layer, or in other words, the length of the concentration gradient region). Consequently, the diffusion layer formed during a 1 s pulse requires roughly 1 s to recover. With the pulsed stripping experiment results suggesting a 2 - 5 s interfacial recovery time after a 1 s current pulse, the remaining recovery process should then be the phase separation recovery, mainly re-alloying of precipitated K metal into NaK. The pulsed stripping experiment showed no significant critical stripping capacity increase as the resting period extends from 5 s to 10 s, seemingly suggesting that the K-NaK re-alloying also completes within 5 s. However, our *operando* DRT spectra collected over the resting period after current scanning (Figure 3c) demonstrates that there's a much slower γ_{int} recovery proceeding between 35 s - 1 h upon resting, suggesting that K-NaK re-alloying takes significantly longer time than phase separation. This is likely the reason that the stripping capacity did not further increase with resting period extended from 5 s to 10 s. Similar slow alloying behavior was reported before in a study on K-Na alloying

View Article Online
DOI: 10.1039/D5EB00097A

process, with the conclusion that NaK formation via K metal alloying into Na metal has significant kinetic barrier,[46] similar barrier may present during K-NaK alloying process. The Na concentration gradient development near the NaK/NASICON interface is the limiting factor for Na stripping from NaK liquid anodes when the current density goes above 0.6 mA/cm^2. Above this limiting current density, the reduced interfacial Na concentration resulted in higher charge transfer resistance, at the same time led to increased interfacial voids as a result of both mechanical deformation and liquid-solid phase separation. These effects in combination resulting in contact loss. Such interfacial degradations are reversible but require an extended resting period to self-recover.

Interfacial Na metal accumulation upon plating

A SGEIS-OCV resting experiment during Na plating (Figure 5a , original EIS spectra provided in Figure **??**.) was conducted on NaK50 liquid electrode. The cell voltage response upon current scanning is near-linear, suggesting that Na plating process is stable and consistent regardless of plating current density. *Operando* DRT spectra, however, show that while γ_{GB} remained unchanged, γ_{int} continuously decreased as the current density increased (Figure 5b). This contradicts with the concentration-dictated alloying observation. Such observations suggest that although Na stripping from NaK is limited by interfacial Na concentration gradient, Na plating is not. As NaK conducts electrons, Na ions from NASICON electrolyte are directly reduced at the interface. When the Na plating rate exceeds the Na-NaK alloying rate in NaK, Na metal can directly precipitate at the NaK/NASICON interface. Precipitated Na metal partially compensates the pre-existing interfacial voids (Figure 5d), reducing mechanical constrictions and therefore decreasing γ_{int}.

During the OCV resting period after the plating current scanning process completed, γ_{int} gradually increased its amplitude between 35 s - 15 h (Figure 5c). Such slow recovery suggests that the precipitated Na metal alloys very slowly with the NaK liquid anode. To confirm this observation, we assembled a K metal/NASICON/Na cell and performed a Na

View Article Online
DOI: 10.1039/D5EB00097A

plating GEIS-OCV resting experiment (Figure **??**), where 0.2 mAh/cm^2 of Na metal is plated into the K metal working electrode. Similarly, we observed immediately reduced γ_{int} upon Na plating, indicating interfacial Na precipitation rather than Na-K alloying process. Upon resting, γ_{int} similarly recovered to pristine level over a 15 h resting period (Figure **??**). Given the slow Na-NaK alloying dynamics, Na metal would quickly accumulate at the NaK/NASICON interface upon Na plating, and eventually lead to Na filament growth and electrolyte penetration failure, similar to solid Na metal anodes. In particular, if a Na plating step follows a Na stripping step without imposing an extended resting period for the stripping-induced contact loss to recover, Na metal precipitation during plating would be highly heterogeneous and lead to very fast cell failure, which is our observation during the CCD test and our *in situ* XCT during Na plating (Figure 1 and Figure 2).

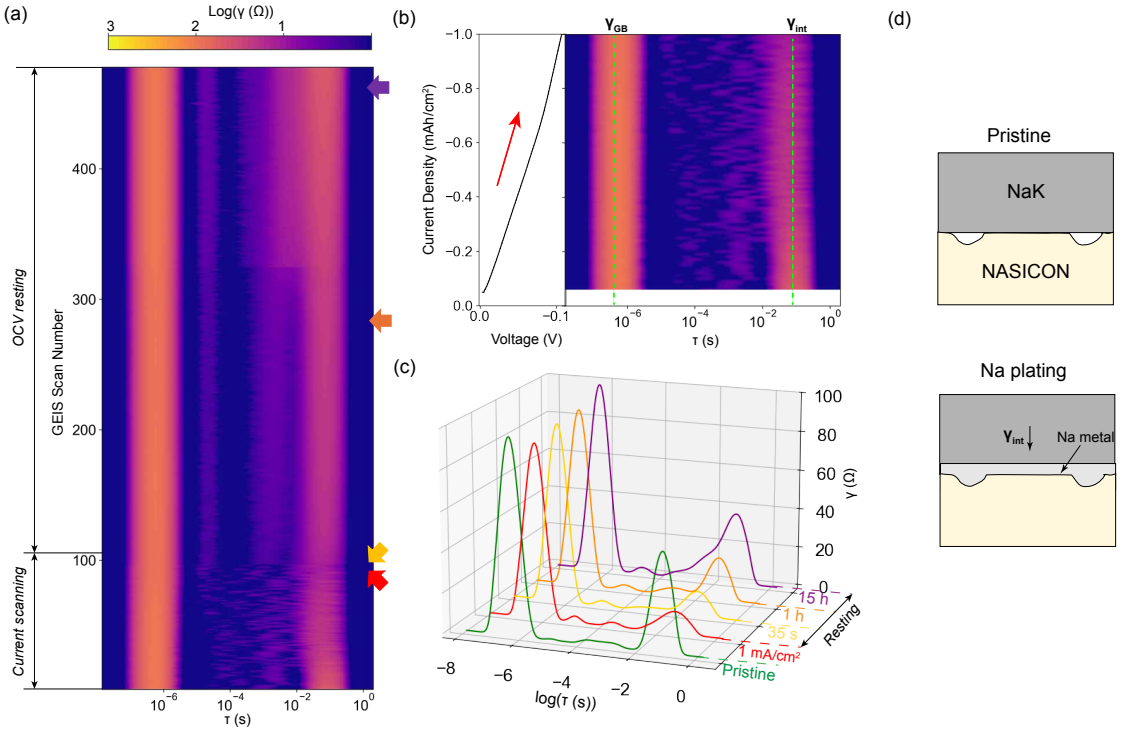

Figure 5: (a) *Operando* DRT spectra obtained during Na plating SGEIS (current scanning) experiment on NaK50 liquid working electrode, followed by an extended resting period. (b) The voltage profile of the SGEIS test and corresponding DRT spectra as functions of Na stripping current density. (c) DRT spectra overlay during current scanning and OCV resting period. (d) Schematics of the NaK/NASICON interface at pristine state, and upon Na plating.

View Article Online
DOI: 10.1039/D5EB00097A

Conclusions

Our experimental results show that the NaK liquid anode is unstable under high Na stripping and plating currents due to different chemo-mechanical degradation processes at the anode-electrolyte interface. The measured Na stripping current limited is ~ 0.6 mA/cm^2 from our SGEIS experiments. This limit is a result of developing Na concentration gradient at the NaK/NASICON interface. We note that this current density is based on geometric contact area, and the real contact area between NaK and NASICON is likely smaller as NaK does not wet NASICON surface. The concentration gradient originates from limited Na diffusion rate inside NaK, and local Na depletion leads to liquid-solid phase transformation and voiding events that effectively cause contact loss. Such degradations, however, can be significantly mitigated by adopting a pulse-stripping protocol, where a Na stripping current pulse is followed by an OCV resting period slightly longer than the pulse duration. This fast self-healing property is due to the fast deformation mechanics of the liquid, as well as relatively fast Na diffusion rate in NaK liquid, compared to in solid metals. The Na plating process is limited by the amount of Na accumulation at the NaK/NASICON interface, thus can be affected by the battery cycling protocol, the applied current density, and the amount of Na deposition. Overall, repeated cycling, high plating current and increased Na plating capacity would all lead to interfacial Na accumulation, followed by Na filament growth and electrolyte penetration failure. Our results show that the anode-electrolyte interfacial contact issue in SSSBs cannot be simply resolved by replacing Na metal with liquid NaK alloys, as the high surface tension of the NaK liquid leads to poor wetting on the electrolyte surface. The non-wetting anode-electrolyte interface significantly limited the contact area, causing local current focusing and lead to increased charge transfer resistance and liquid-solid phase separation, which eventually accelerated anode-electrolyte failure. This study elucidated that the NaK/NASICON interfacial degradations are mainly induced by inhomogeneous anode-electrolyte contact, and subsequent chemo-mechanical degradation due to interfacial Na depletion (stripping) or Na accumulation (plating). With the above

View Article Online
DOI: 10.1039/D5EB00097A

conclusions in mind, the practical value of NaK anodes and the pathway toward its real world applications become clear. Compared to solid metal anodes for SSBs, liquid NaK anode enables very fast and thorough chemo-mechanical self-recovery of the interface *via* liquid flow and facile Na diffusion. Therefore, those degradations are self-recoverable by adopting a pulsed current charge/discharge during battery operation, which resembles the duty cycle of real battery packs,[47] and is achievable via battery pack-level engineering in real-world applications. Furthermore, the interfacial degradations can be significantly mitigated with a wetting anode-electrolyte interface between NaK liquid and NASICON electrolyte. This can be achieved by either reducing the surface tension of NaK liquids with additives,[18] or engineering a surface coating layer on NASICON electrolytes.[23] The above strategies would help NaK anodes achieve realistic cycling current densities.

Acknowledgement

This work was primarily funded by the U.S. Department of Energy (DOE) under grant DE-SC0023462. This research used resources of the National Synchrotron Light Source II, a DOE Office of Science user facility operated for the DOE Office of Science by Brookhaven National Laboratory. X-ray imaging experiments was funded by the Energy Storage Research Alliance "ESRA" (DE-AC02-06CH11357), an Energy Innovation Hub funded by the U.S. Department of Energy, Office of Science, Basic Energy Sciences. The authors acknowledge the use of the Imaging and Analysis Center (IAC) operated by the Princeton Materials Institute at Princeton University, which is supported in part by the Princeton Center for Complex Materials (PCCM), a National Science Foundation (NSF) Materials Research Science and Engineering Center (MRSEC; DMR-2011750).

View Article Online
DOI: 10.1039/D5EB00097A

References

(1) Wu, D.; Alsaç, E. P.; Claus, A.; Fang, Z.; Jangid, M. K.; Lee, K.; Nelson, D. L.; Park, S. H.; Zhang, S.; Chi, M.; others The State of Reliable Characterization and Testing of Solid-State Batteries. *ACS Energy Letters* **2025**, *10*, 2617–2630.

(2) Zhou, C.; Bag, S.; Thangadurai, V. Engineering Materials for Progressive All-Solid-State Na Batteries. *ACS Energy Letters* **2018**, *3*, 2181–2198.

(3) Zhao, C.; Liu, L.; Qi, X.; Lu, Y.; Wu, F.; Zhao, J.; Yu, Y.; Hu, Y.-S.; Chen, L. Solid-State Sodium Batteries. *Advanced Energy Materials* **2018**, *8*, 1703012.

(4) Janek, J.; Zeier, W. G. Challenges in speeding up solid-state battery development. *Nature Energy* **2023**, *8*, 230–240.

(5) Zaman, W.; Zhao, L.; Martin, T.; Zhang, X.; Wang, Z.; Wang, Q. J.; Harris, S.; Hatzell, K. B. Temperature and pressure effects on unrecoverable voids in Li metal solid-state batteries. *ACS Applied Materials & Interfaces* **2023**, *15*, 37401–37409.

(6) Ren, Y.; Hortance, N.; Hatzell, K. B. Mitigating chemo-mechanical failure in Li-S solid state batteries with compliant cathodes. *Journal of The Electrochemical Society* **2022**, *169*, 060503.

(7) Kasemchainan, J.; Zekoll, S.; Spencer Jolly, D.; Ning, Z.; Hartley, G. O.; Marrow, J.; Bruce, P. G. Critical stripping current leads to dendrite formation on plating in lithium anode solid electrolyte cells. *Nature materials* **2019**, *18*, 1105–1111.

(8) Dixit, M. B.; Verma, A.; Zaman, W.; Zhong, X.; Kenesei, P.; Park, J. S.; Almer, J.; Mukherjee, P. P.; Hatzell, K. B. Synchrotron imaging of pore formation in Li metal solid-state batteries aided by machine learning. *ACS Applied Energy Materials* **2020**, *3*, 9534–9542.

View Article Online
DOI: 10.1039/D5EB00097A

(9) Lee, K.; Sakamoto, J. Effect of depth of discharge (DOD) on cycling in situ formed Li anodes. *Faraday Discuss.* **2024**, *248*, 250–265.

(10) Lin, L.; Ayyaswamy, A.; Zheng, Y.; Fan, A.; Vishnugopi, B. S.; Mukherjee, P. P.; Hatzell, K. B. Nonintuitive role of solid electrolyte porosity on failure. *ACS Energy Letters* **2024**, *9*, 2387–2393.

(11) Park, S. H.; Ayyaswamy, A.; Gjerde, J.; Andrews, W. B.; Vishnugopi, B. S.; Drakopoulos, M.; Vo, N. T.; Zhong, Z.; Thornton, K.; Mukherjee, P. P.; others Filament-Induced Failure in Lithium-Reservoir-Free Solid-State Batteries. *ACS Energy Letters* **2025**, *10*, 1174–1182.

(12) Park, S. H.; Naik, K. G.; Vishnugopi, B. S.; Mukherjee, P. P.; Hatzell, K. B. Lithium Kinetics in Ag–C Porous Interlayer in Reservoir-Free Solid-State Batteries. *Advanced Energy Materials* **2025**, *15*, 2405129.

(13) Cheng, Y.; Li, M.; Yang, X.; Lu, X.; Wu, D.; Zhang, Q.; Zhu, Y.; Gu, M. Na–K Alloy Anode for High-Performance Solid-State Sodium Metal Batteries. *Nano Letters* **2022**, *22*, 9614–9620, Publisher: American Chemical Society.

(14) Guo, X.; Bae, J.; Ding, Y.; Zhang, X.; Yu, G. Liquid Alloy Enabled Solid-State Batteries for Conformal Electrode–Electrolyte Interfaces. *Advanced Functional Materials* **2021**, *31*, 2010863, _eprint: https://onlinelibrary.wiley.com/doi/pdf/10.1002/adfm.202010863.

(15) Leonchuk, S. S.; Falchevskaya, A. S.; Nikolaev, V.; Vinogradov, V. V. NaK alloy: underrated liquid metal. *J. Mater. Chem. A* **2022**, *10*, 22955–22976.

(16) Xue, L.; Zhou, W.; Xin, S.; Gao, H.; Li, Y.; Zhou, A.; Goodenough, J. B. Room-Temperature Liquid Na–K Anode Membranes. *Angewandte Chemie International Edition* **2018**, *57*, 14184–14187.

View Article Online
DOI: 10.1039/D5EB00097A

(17) Liu, C. et al. Liquid Alloying Na–K for Sodium Metal Anodes. *The Journal of Physical Chemistry Letters* **2021**, *12*, 9321–9327, PMID: 34544240.

(18) Zhang, L.; Li, Y.; Zhang, S.; Wang, X.; Xia, X.; Xie, D.; Gu, C.; Tu, J. Non-Newtonian Fluid State K–Na Alloy for a Stretchable Energy Storage Device. *Small Methods* **2019**, *3*, 1900383.

(19) Koh, H.; Hassan, M. H.; Lin, S.; Wang, L.; Stach, E. A.; Detsi, E. Liquid Na-K alloy is not viable anode material for High-Performance Na-Ion batteries. *Chemical Engineering Journal* **2024**, *490*, 151578.

(20) Zhang, L.; Peng, S.; Ding, Y.; Guo, X.; Qian, Y.; Celio, H.; He, G.; Yu, G. A graphite intercalation compound associated with liquid Na–K towards ultra-stable and high-capacity alkali metal anodes. *Energy Environ. Sci.* **2019**, *12*, 1989–1998.

(21) Suo, J.; Zhao, Q.; Tian, H.; Wang, L.; Dai, L.; Luo, J.; Liu, S. Designing a Quasi-Liquid Alloy Interface for Solid Na-Ion Battery. *ACS Nano* **2023**, *17*, 10229–10235, Publisher: American Chemical Society.

(22) Tian, H.; Liu, S.; Deng, L.; Wang, L.; Dai, L. New-type Hf-based NASICON electrolyte for solid-state Na-ion batteries with superior long-cycling stability and rate capability. *Energy Storage Materials* **2021**, *39*, 232–238.

(23) Guo, X.; Liu, Y.; Zhang, X.; Ju, Z.; Li, Y.; Mitlin, D.; Yu, G. Revealing the Solid-State Electrolyte Interfacial Stability Model with Na–K Liquid Alloy. *Angewandte Chemie International Edition* **2022**, *61*, e202203409, _eprint: https://onlinelibrary.wiley.com/doi/pdf/10.1002/anie.202203409.

(24) Ortmann, T.; Burkhardt, S.; Eckhardt, J. K.; Fuchs, T.; Ding, Z.; Sann, J.; Rohnke, M.; Ma, Q.; Tietz, F.; Fattakhova-Rohlfing, D.; Kübel, C.; Guillon, O.; Heiliger, C.; Janek, J. Kinetics and Pore Formation of the Sodium

View Article Online
DOI: 10.1039/D5EB00097A

Metal Anode on NASICON-Type Na3.4Zr2Si2.4P0.6O12 for Sodium Solid-State Batteries. *Advanced Energy Materials* **2023**, *13*, 2202712, _eprint: https://onlinelibrary.wiley.com/doi/pdf/10.1002/aenm.202202712.

(25) Drakopoulos, M.; Zhong, Z.; Vo, N.; Broadbent, A.; Lucas, M. HEX: A New High Energy Beamline at NSLS-II. *Synchrotron Radiation News* **2024**, *37*, 50–51.

(26) Vo, N. T.; Atwood, R. C.; Drakopoulos, M.; Connolley, T. Data processing methods and data acquisition for samples larger than the field of view in parallel-beam tomography. *Opt. Express* **2021**, *29*, 17849–17874.

(27) Vo, N. T.; Atwood, R. C.; Drakopoulos, M. Superior techniques for eliminating ring artifacts in X-ray micro-tomography. *Opt. Express* **2018**, *26*, 28396–28412.

(28) Eckhardt, J. K.; Klar, P. J.; Janek, J.; Heiliger, C. Interplay of Dynamic Constriction and Interface Morphology between Reversible Metal Anode and Solid Electrolyte in Solid State Batteries. *ACS Applied Materials & Interfaces* **2022**, *14*, 35545–35554, Publisher: American Chemical Society.

(29) Gross, M. M.; Small, L. J.; Peretti, A. S.; Percival, S. J.; Rodriguez, M. A.; Spoerke, E. D. Tin-based ionic chaperone phases to improve low temperature molten sodium–NaSICON interfaces. *J. Mater. Chem. A* **2020**, *8*, 17012–17018.

(30) Xue, L.; Gao, H.; Zhou, W.; Xin, S.; Park, K.; Li, Y.; Goodenough, J. B. Liquid K–Na Alloy Anode Enables Dendrite-Free Potassium Batteries. *Advanced Materials* **2016**, *28*, 9608–9612.

(31) Huang, M.; Xi, B.; Feng, Z.; Wu, F.; Wei, D.; Liu, J.; Feng, J.; Qian, Y.; Xiong, S. New Insights into the Electrochemistry Superiority of Liquid Na–K Alloy in Metal Batteries. *Small* **2019**, *15*, 1804916.

View Article Online
DOI: 10.1039/D5EB00097A

(32) Dixit, M. B.; Singh, N.; Horwath, J. P.; Shevchenko, P. D.; Jones, M.; Stach, E. A.; Arthur, T. S.; Hatzell, K. B. In situ investigation of chemomechanical effects in thiophosphate solid electrolytes. *Matter* **2020**, *3*, 2138–2159.

(33) Sandoval, S. E.; Haslam, C. G.; Vishnugopi, B. S.; Liao, D. W.; Yoon, J. S.; Park, S. H.; Wang, Y.; Mitlin, D.; Hatzell, K. B.; Siegel, D. J.; others Electro-chemo-mechanics of anode-free solid-state batteries. *Nature Materials* **2025**, 1–9.

(34) Seitzman, N.; Bird, O. F.; Andrykowski, R.; Robbins, S.; Al-Jassim, M. M.; Pylypenko, S. Operando X-ray tomography imaging of solid-state electrolyte response to Li evolution under realistic operating conditions. *ACS Applied Energy Materials* **2021**, *4*, 1346–1355.

(35) Hao, S.; Daemi, S. R.; Heenan, T. M. M.; Du, W.; Tan, C.; Storm, M.; Rau, C.; Brett, D. J. L.; Shearing, P. R. Tracking lithium penetration in solid electrolytes in 3D by in-situ synchrotron X-ray computed tomography. *Nano Energy* **2021**, *82*, 105744.

(36) Ning, Z.; Li, G.; Melvin, D. L.; Chen, Y.; Bu, J.; Spencer-Jolly, D.; Liu, J.; Hu, B.; Gao, X.; Perera, J.; others Dendrite initiation and propagation in lithium metal solid-state batteries. *Nature* **2023**, *618*, 287–293.

(37) Wu, D.; Li, Z.; Drakopoulos, M.; Vo, N. T.; Zhong, Z.; Hatzell, K. B. Phase separation dynamics in sodium solid-state batteries with Na–K liquid anodes. *J. Mater. Chem. A* **2025**, *13*, 22074–22085.

(38) Bard, A. J.; Faulkner, L. R.; White, H. S. *Electrochemical methods: fundamentals and applications*; John Wiley & Sons, 2022.

(39) Haslam, C. G.; Eckhardt, J. K.; Ayyaswamy, A.; Vishnugopi, B. S.; Fuchs, T.; Liao, D. W.; Dasgupta, N. P.; Mukherjee, P. P.; Janek, J.; Sakamoto, J. Evaluating Pressure-dependent Discharge Behavior of Foil Versus In situ Plated Lithium Metal Anodes in Solid-State Batteries. *Advanced Energy Materials* **2024**, *n/a*, 2403614.

View Article Online
DOI: 10.1039/D5EB00097A

(40) Lee, K.; Kazyak, E.; Wang, M. J.; Dasgupta, N. P.; Sakamoto, J. Analyzing void formation and rewetting of thin in situ-formed Li anodes on LLZO. *Joule* **2022**, *6*, 2547–2565.

(41) Liao, J.; Majidi, C.; Sitti, M. Liquid Metal Actuators: A Comparative Analysis of Surface Tension Controlled Actuation. *Advanced Materials* **2024**, *36*, 2300560.

(42) Bansal, S.; Tokuda, Y.; Peasley, J.; Subramanian, S. Electrically Induced Liquid Metal Droplet Bouncing. *Langmuir* **2022**, *38*, 6996–7004, PMID: 35617048.

(43) Wang, S.; Zhang, Y.; Wang, J.; Ren, D.; Yu, Z. Electrically driven heartbeat effect of gallium-based liquid metal on a ratchet. *Frontiers in Bioengineering and Biotechnology* **2023**, *Volume 10 - 2022*.

(44) Tang, S.-Y.; Sivan, V.; Petersen, P.; Zhang, W.; Morrison, P. D.; Kalantar-zadeh, K.; Mitchell, A.; Khoshmanesh, K. Liquid Metal Actuator for Inducing Chaotic Advection. *Advanced Functional Materials* **2014**, *24*, 5851–5858.

(45) Wissman, J.; Dickey, M. D.; Majidi, C. Field-Controlled Electrical Switch with Liquid Metal. *Advanced Science* **2017**, *4*, 1700169.

(46) Wang, H.; Li, Y.; Luo, Y.; Yuan, W.; Chen, X.; Zhang, L.; Shu, J. Expounding the Initial Alloying Behavior of Na–K Liquid Alloy Electrodes. *ACS Applied Materials & Interfaces* **2021**, *13*, 40118–40126, Publisher: American Chemical Society.

(47) Lee, K.; Sakamoto, J. Li Stripping Behavior of Anode-Free Solid-State Batteries Under Intermittent-Current Discharge Conditions. *Advanced Energy Materials* **2024**, *14*, 2303571.

View Article Online
DOI: 10.1039/D5EB00097A

The data that support the findings of this study are available from the corresponding author upon reasonable request. All relevant experimental data, analysis scripts, and processed datasets used in generating the figures are available in the supplementary information and/or will be deposited in an open-access repository [e.g., Zenodo, Figshare] upon publication.